Proposal for atom traps with low power by surface plasmon polaritons on the short waveguide

Aiping Liu [1,2,3,4,*] Zhanfei Kang,[1,3,4] Tong Wang,[1,3] Pengfei Zhang,[2] Xifeng Ren,[4,5,6]
Chang-Ling Zou,[4,5,6,†] and Qin Wang [1,3]

[1]*Key Laboratory of Broadband Wireless Communication and Sensor Network Technology, Ministry of Education,*
Nanjing University of Posts and Telecommunications, Nanjing 210003, China
[2]*State Key Laboratory of Quantum Optics and Quantum Optics Devices and Institute of Opto-Electronics,*
Shanxi University, Taiyuan 030006, China
[3]*Institute of Quantum Information and Technology, Nanjing University of Posts and Telecommunications, Nanjing 210003, China*
[4]*Hefei National Laboratory, University of Science and Technology of China, Hefei 230088, China*
[5]*CAS Key Laboratory of Quantum Information, University of Science and Technology of China, Hefei 230026, China*
[6]*CAS Center for Excellence in Quantum Information and Quantum Physics,*
University of Science and Technology of China, Hefei 230026, China

In this study, a viable platform for atom traps using a dielectric-loaded surface-plasmon-polariton waveguide is proposed. A trap depth of 0.239 mK can be achieved above a SiO_2 waveguide on an Au-SiO_2 substrate, with mode powers of 0.5 mW for the blue-detuned TM_0 mode, 0.1 mW for the TM_1 mode, and 0.55 mW for the red-detuned TM_0 mode. The trap center is about 180 nm above the waveguide surface, and the corresponding cooperativity parameter for coupling the ^{87}Rb atom with a guided photon is about 0.137. By controlling the phase difference between counterpropagating red-detuned TM_0 modes, atoms can be delivered along the waveguide by an optical conveyor belt. Compared to the dielectric waveguide without the enhancement of surface plasmon polaritons, our scheme has the advantage of forming a trap depth with low-power requirements and stronger atom-photon interactions, which makes it highly suitable for applications in photonic-atomic chips.

I. INTRODUCTION

Due to their high scalability and improved light-matter interaction, integrated quantum photonic chips have garnered significant attention in recent decades [1–3]. There is a growing demand for quantum photonic devices with single emitters, which are essential for quantum light sources, single-photon-level nonlinearity, and deterministic quantum gate operations [4–6]. Neutral atoms with long-lived energy levels also have the potential to serve as long coherence time memory for storing quantum information [7,8]. Therefore, integrated photonic-atomic chips based on neutral atoms offer promising prospects and have attracted considerable effort, especially for atom trapping and manipulation in recent years [9–14].

Various technologies, such as nanofibers [15–17], two-dimensional periodic optical structures for atom lattice arrays [18,19], nano-optical tweezers [20–22], microring resonators [23–25], and rib waveguides [26–28], have been employed for atom trapping and manipulation. However, many of these platforms necessitate high light power for effective atom trapping, leading to increased experimental complexity and instability in trapping atoms. Surface plasmon polaritons (SPPs) are collective oscillation waves of electrons that are beyond the diffraction limit and propagate along the interface of the metal and dielectric [29–32]. Although the trapping of atoms with SPPs has been studied [19,33–35], atom traps on waveguides with SPPs are still absent. Our proposal involves utilizing a hybrid waveguide assisted by SPPs to effectively reduce the required power for trapping atoms in a short range. This platform has the potential to offer a stable atom source for integrated photonic-atomic chips.

In this paper, a platform composed of a SiO_2 waveguide on an Au-SiO_2 substrate is proposed for ^{87}Rb atom traps with low power assisted by SPPs. A trap depth of about 0.239 mK can be achieved above the waveguide, where the powers of the blue-detuned TM_0 mode, the TM_1 mode, and the red-detuned TM_0 mode are 0.5, 0.1, and 0.55 mW, respectively. The trap center is about 180 nm above the waveguide surface with a cooperativity parameter being about 0.137. Compared to conventional dielectric waveguide or SPP waveguides based on Si_3N_4, the SiO_2 on Au-SiO_2 platform can provide a similar trap depth with a lower mode power but a larger cooperativity parameter in a short range. The proposed platform offers an alternative approach for trapping atoms with low power and strong atom-photon coupling for integrated photonic-atomic chips.

The paper is organized as follows. Section II provides an overview of the platform for atom traps with SPP modes. Section III gives a comparison of different platforms. Section IV demonstrates the performance of the SiO_2 on Au-SiO_2 form for atom traps. A summary is given in Sec. V.

*Contact author: apliu@njupt.edu.cn
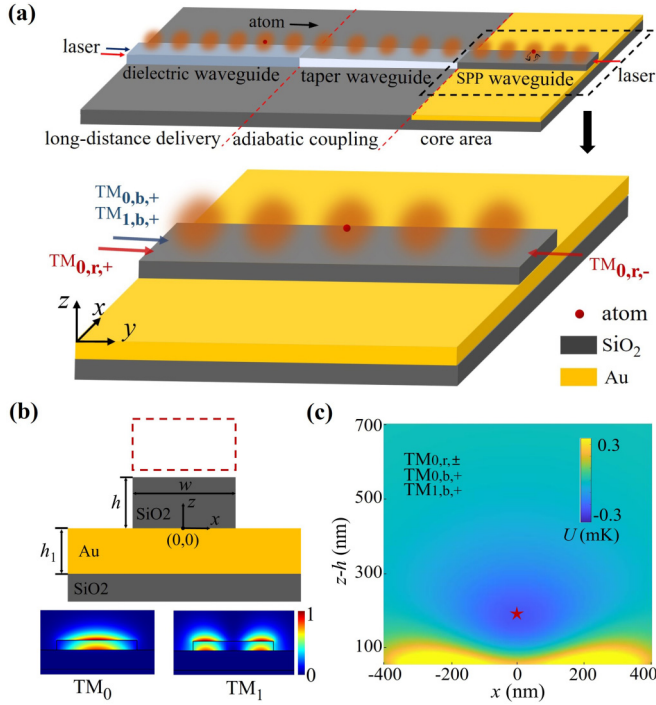†Contact author: clzou321@ustc.edu.cn

FIG. 1. (a) Schematic of the photonic-atomic chip device for atom trapping and delivery, which includes a dielectric waveguide, tapering region, and SPP waveguide. The inset is the SPP waveguide for atom trapping and delivery. (b) Cross section of the waveguide and the electric-field distributions of the TM_0 and TM_1 modes. (c) Trap potential distribution above the waveguide surface in the x-z plane shown by the red dashed rectangle in (b).

II. PLATFORM FOR AN ATOM TRAP WITH SPP MODES

The photonic-atomic chip platform depicted in Fig. 1(a) comprises a SiO_2 waveguide on an Au-SiO_2 substrate, which forms a dielectric-loaded SPP waveguide. As illustrated in Fig. 1(b), the SiO_2 waveguide is characterized by width w and height h, and the Au film with a thickness of $h_1 = 200$ nm is deposited on a SiO_2 substrate. The SPPs at the interface between the dielectric waveguide and the Au can be excited, confined, and guided in the waveguide. It is noteworthy that the evanescent field attenuates exponentially from the surface of the waveguide, thereby providing repulsion and attraction to the atom with the blue- and red-detuned modes, respectively [33,34]. Additionally, when atoms approach the waveguide surface, surface interactions exert a rapidly increasing attractive force due to van der Waals force or Casimir-Polder force, depending on the atom-surface distance l and the transition wavelength λ of the atoms [36–38]. To counteract the van der Waals or Casimir-Polder force and prevent the atom from adhering to the waveguide surface, the blue-detuned TM_0 and TM_1 modes are employed to provide a repulsive force. It is important to highlight that only TM modes can be induced on the dielectric-loading SPP waveguide, in contrast to dielectric waveguides that support both TE and TM modes. Consequently, only the evanescent field associated with TM modes is taken into account when calculating the optical dipole potential. As illustrated in Fig. 1(a), for $w = 800$ nm and $h = 100$ nm and considering the ^{87}Rb atom
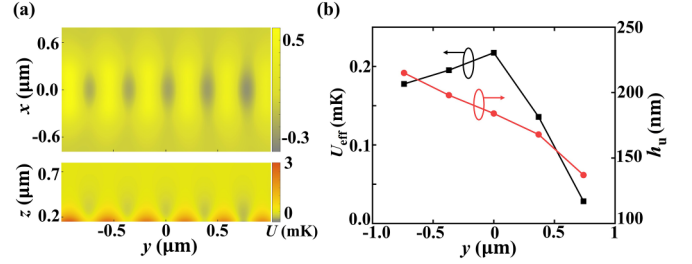

FIG. 2. Trap potential formed along the waveguide with mode input powers of $P_b = 0.606$ mW, $P_{b1} = 0.130$ mW, and $P_r = 0.630$ mW. (a) Trap potential distribution in the x-y plane 180 nm above the waveguide surface (top) and in the y-z plane with $x = 0$ (bottom). (b) Variation of the trap depth and the trap center along the waveguide.

with a D_2 transition at the wavelength $\lambda_0 = 780$ nm, TM_0 and TM_1 modes are excited by blue-detuned lasers, with $\lambda = 760$ and 765 nm, respectively. The optical constants of Si_3N_4 and Au are obtained from Refs. [39,40], and the refractive index of SiO_2 is set equal to 1.45 [41]. By the finite-element method, the SPP modes are calculated on the dielectric-loading SPP waveguide. The electric-field distributions of the TM_0 mode for $\lambda = 760$ nm and TM_1 mode for $\lambda = 765$ nm are given in Fig. 1(b). Another red-detuned laser ($\lambda = 850$ nm) is used to excite the TM_0 mode for attractive forces, and thus the combinations of all the dipole lasers and surface forces lead to an atom trap potential well above the waveguide.

Figure 1(c) shows the trap potential distribution on the x-z plane above the waveguide surface [corresponding to the red rectangular area in Fig. 1(b)], where the powers of the $TM_{0,b,+}$ and $TM_{1,b,+}$ modes are $P_b = 0.5$ mW and $P_{b1} = 0.1$ mW, respectively, and the power of the $TM_{0,r,\pm}$ mode in one direction is $P_r = 0.55$ mW. The subscripts $+$ and $-$ indicate the forward and backward excitation directions, respectively. Here the trap potential is calculated by the formulas according to Refs. [23,33,34,42]. Since the distance between the trap center and waveguide surface is larger than $\lambda/2\pi$, the Casimir-Polder potential is considered in the calculation of the trap potential [38,43]. Note that the blue-detuned TM_0 and TM_1 modes propagate unidirectionally, while the counterpropagating red-detuned TM_0 modes are excited simultaneously to form a standing-wave potential for the atom conveyor belt [23]. The trap center (denoted by a red star) is about 180 nm above the waveguide surface (denoted by h_u). The saddle of the trap well is infinity and is not shown in the figure. The trap depth U_{eff} (difference between the trap center and the saddle) is approximately 0.239 mK. The trapping frequencies of the ^{87}Rb atom in the trap well are $2\pi \times 0.14$, $2\pi \times 0.44$, and $2\pi \times 0.25$ MHz in the x, y, and z directions, respectively, and the corresponding oscillation energies are 6.84, 21.24, and 12.05 µK, which are much smaller than the trap depth.

Figure 2(a) illustrates the optical trap potential in the x-y plane positioned 180 nm above the waveguide surface and in the y-z plane with $x = 0$. Limited to the large losses and short propagation length of the SPP, a short range of 3 µm is considered to analyze the atom trapping on the waveguide. The sources of the forward $TM_{0,b,+}$, $TM_{1,b,+}$, and $TM_{0,r,+}$ modes are positioned at $y = -1.5$ µm and have powers of

TABLE I. Performance of different platforms for trapping atoms. Here h_u is the distance of the trap center from the waveguide surface.

Waveguides	SiO$_2$ on Au-SiO$_2$	Si$_3$N$_4$ on Au-SiO$_2$	Si$_3$N$_4$ on SiO$_2$
h (nm)	100	100	280
w (nm)	800	800	800
P_b (mW)	0.5	1.2	9
P_{b1} (mW)	0.1	0.3	1
P_r (mW)	0.55	0.828	9.36
U_{eff} (mK)	0.239	0.238	0.237
h_u (nm)	180	130	135
C	0.137	0.049	0.021
$L_{TM_{0,r}}$ (μm)	13.12	3.73	222198
$L_{TM_{0,b}}$ (μm)	8.27	2.6	5234
$L_{TM_{1,b}}$ (μm)	8.64	2.54	13256

0.606, 0.130, and 0.630 mW, respectively. The source of the backward $TM_{0,r,-}$ mode is positioned at $y = 1.5$ μm with a power of 0.630 mW. By adjusting the phase difference between the two $TM_{0,r,\pm}$ modes, the optical trap lattice can move and transport trapped atoms along the waveguide surface. Owing to propagation loss, the trap depth U_{eff} and the trap center h_u vary as the guiding modes propagate along the waveguide, as shown in Fig. 2(b). The trap depth first increases and subsequently decreases rapidly in the forward direction, as indicated by the black curve. Simultaneously, the trap center approaches the waveguide surface in the forward direction, as shown by the red curve. It should be noted that the length of the waveguide is not limited to 3 μm, since the propagation length of SPP modes is beyond 8 μm. The optical trap potential given in Fig. 2(a) can be obtained when the incident power of $TM_{0,r,-}$ is high enough to overcome the propagation loss. Loading atoms into the trap well formed on the unsuspended dielectric-loading SPP waveguide presents additional challenges due to the presence of the reflective Au film. Several approaches have been explored in previous studies to address this issue and successfully load atoms into the trap well on unsuspended waveguides. These methods include using counterpropagating lasers perpendicular to the waveguide surface [44], leveraging the strong near field generated by a sharp metallic nanotip for trapping and delivering atoms [33], and employing grating diffraction beams at the Brewster angle to mitigate reflections [45]. Therefore, it is feasible to load atoms into the trap well on the dielectric-loading SPP waveguide.

III. COMPARISON OF DIFFERENT PLATFORMS

To compare with other photonic-atomic chip schemes, trap depths formed by a Si$_3$N$_4$ waveguide on SiO$_2$ substrate and a Si$_3$N$_4$ waveguide on Au-SiO$_2$ substrate are studied, as presented in Table I. The Si$_3$N$_4$ on Au-SiO$_2$ platform provides better confinement, where more mode fields are distributed inside the Si$_3$N$_4$ waveguide due to the larger refractive index of Si$_3$N$_4$ than that of SiO$_2$. With the powers of the $TM_{0,b}$, $TM_{1,b}$, and $TM_{0,r}$ modes set equal to 1.2, 0.3, and 0.828 mW, respectively, a trap depth of 0.238 mK can be obtained with a trap center of $h_u \sim 130$ nm. The Si$_3$N$_4$ on SiO$_2$ platform provides an example of a conventional dielectric waveguide,

and the waveguide height is designed with $h = 280$ nm, which is larger than that of the SPP cases because of the limit of optical confinement in a dielectric waveguide. The powers required for a trap depth of 0.237 mK are $P_b = 9$ mW, $P_{b1} = 1$ mW, and $P_r = 9.36$ mW, with the trap center located at $h_u \sim 135$ nm. These results indicate that the SPP can significantly reduce the optical power requirement by about one order of magnitude, while a relatively low refractive index of dielectric loading is preferable due to loose confinement of light for a stronger evanescent field in vacuum.

Due to the absorption loss in the Au film, the intensity of the SPP mode decays with propagation distance as $I \sim \exp(-y/L)$, where L represents the mode propagation length in the waveguide. The calculated propagation lengths of the $TM_{0,b}$, $TM_{1,b}$, and $TM_{0,r}$ modes are also given in Table I. The SiO$_2$-based SPP waveguide outperforms the Si$_3$N$_4$-based SPP waveguide, confirming the weaker confinement provided by the low-index dielectric materials. In contrast to the Si$_3$N$_4$ on SiO$_2$ platform, which offers waveguide modes with a long propagation length, the SiO$_2$-loaded SPP waveguide is constrained by short propagation lengths of approximately 10 μm. With a short propagation length, SPP modes can be applied to trap atoms in the core area of atomic chip. The SPP waveguide and dielectric waveguide can cooperate with each other to realize the manipulation of atoms on the atomic-photonic chip as shown in Fig. 1(a), where a long-distance atomic transmission scheme includes the dielectric waveguide, tapering region, and SPP waveguide. For the long-distance delivery, dielectric waveguide modes with high power can be utilized to transport atoms. When the atoms reach the critical region for interactions, SPP modes can be employed to trap single atoms and transport atoms in a short distance, where the atoms can be held for a long time with low trap power. While the inherent losses of the SPP restricts its applications to a short range, the enhancement of the SPP presents an advantage in atom trapping due to its low-power requirements. In fields such as quantum information processing and high-precision sensing relying on single atoms, susceptibility to temperature variations and environmental disturbances is a critical concern. By utilizing SPP modes for atom trapping with low-power demands, the stability and quality of the system can be significantly improved. It is different from the optical fiber waveguide [16], which has difficulty dissipating the heat with a suspended waveguide; in contrast, the SPP waveguide can dissipate the heat to the substrate by the gold film for good thermal conductivity. Our research offers a promising solution for achieving a stable atom trap on a photonic-atomic chip. Additionally, a growing number of researchers have endeavored to increase the propagation length of SPP modes in recent years. For instance, the Si-SiO$_2$-Au platform was introduced to extend the propagation length of SPP modes to 50–200 μm in the infrared spectrum [46]. In addition, the integration of graphene nanoribbons with electrodes between two dielectric layers in the SiO$_2$-Au waveguide has enabled the extension of the propagation length of SPP modes to 187.9 μm in the terahertz band [47]. These advancements suggest that the limitations of short propagation distances might be improved for SPP modes in the future.

As the atom is trapped above the waveguide surface, the emission of the trapped atom can couple to the waveguide

mode through the evanescent field. The merit of the quantum coherence of the atom-photon interaction on the waveguide for the atom located at the working point (x_0, y_0, z_0) can be determined by the cooperativity parameter as [23]

$$C = \frac{3 n_{\text{eff}} \lambda^2}{4 \pi A_{\text{eff}}} \frac{|E(x_0, y_0, z_0)|}{\max[|E(x, y, z)|]}, \quad (1)$$

where n_{eff} is the effective refractive index, $E(x, y, z)$ is the electric field of the waveguide mode with the origin of the coordinate system at the center of waveguide down surface as shown in Fig. 1(b), and A_{eff} is the effective mode area. For an atom on the straight waveguide,

$$A_{\text{eff}} = \frac{\int \epsilon(x, z) |E(x, z)|^2 dx \, dz}{\epsilon(x_0, z_0) |E(x_0, z_0)|^2}, \quad (2)$$

with ϵ the dielectric permittivity. For the ^{87}Rb atom at the trapped center coupling to the TM$_0$ mode at $\lambda = 780$ nm, the cooperativity parameter for the SiO$_2$ on Au-SiO$_2$ platform is 0.137, which is larger than that of the other two platforms (0.049 and 0.021 for the Si$_3$N$_4$ on Au-SiO$_2$ and Si$_3$N$_4$ on SiO$_2$ platforms), as shown in Table I. This shows that the SiO$_2$ on Au-SiO$_2$ platform provides a higher trap center but a larger cooperativity parameter. The short propagation length of the lossy SPP modes will limit the effective atom-photon interaction. To take advantage of SPP modes for atom trapping and atom-photon interaction, the SPP can be applied only in the critical region of the atomic chip. A tapered waveguide can be used to connect the SPP waveguide with the low-loss dielectric waveguide, which can realize the effective and adiabatic coupling between the SPP mode and dielectric waveguide mode. The calculated transmission efficiency of the TM$_0$ mode at $\lambda = 780$ nm is about 0.7 across the SPP waveguide with a length of 3 μm. To estimate the coupling efficiency between dielectric waveguides and SPP waveguides as 0.5 [48,49], the effective atom-photon coupling efficiency is about 0.048 for the SiO$_2$ on Au-SiO$_2$ platform and 0.017 for the Si$_3$N$_4$ on Au-SiO$_2$ platform. Therefore, the SPP mode based on the SiO$_2$ on Au-SiO$_2$ platform can provide strong atom-photon interactions especially in a short range.

IV. PERFORMANCE OF THE SiO$_2$ ON Au-SiO$_2$ PLATFORM

The subsequent analysis delves further into the atom trap on the SiO$_2$ on Au-SiO$_2$ platform. The trap depth varies with $P_{\text{r}}/P_{\text{b}}$, as shown in Fig. 3, where the waveguide width is $w = 800$ nm and the height is $h = 100$ nm. The relationships between the trap depth and $P_{\text{r}}/P_{\text{b}}$ for different P_{b} and the same $P_{\text{b1}} = 0.1$ mW is illustrated in Fig. 3(a), where the different curves correspond to $P_{\text{b}} = 0.3$, 0.4, 0.5, and 0.6 mW, respectively. With a larger P_{b}, more of the electric field is above the waveguide surface, allowing for the formation of a greater trap depth. For each curve, the trap depth increases initially and then decreases with $P_{\text{r}}/P_{\text{b}}$ to reach a maximum. When $P_{\text{r}}/P_{\text{b}}$ is relatively small, the repulsive force from the blue-detuned light is dominant and substantial. The saddle point (denoted by the red cross) of the trap well is located at infinity, as shown in Fig. 3(b) with $P_{\text{r}}/P_{\text{b}} = 1.05$, $P_{\text{b}} = 0.5$ mW, and $P_{\text{b1}} = 0.1$ mW. As the repulsive force can overcome the absorptive force from red-detuned light and the van de Walls force near the waveguide surface, the trap depth determined by the trap
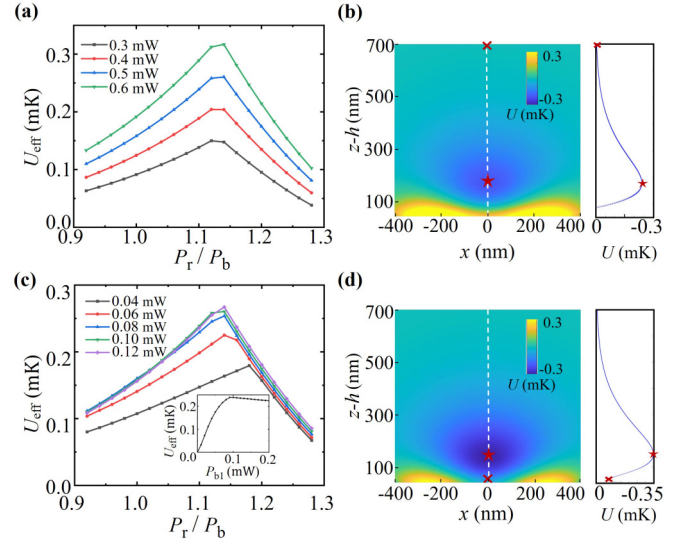

FIG. 3. Relation between the trap depth and $P_{\text{r}}/P_{\text{b}}$, where different lines correspond to different (a) P_{b} and (c) P_{b1}. The inset in (c) shows the relation between the trap depth and P_{b1} with $P_{\text{b}} = 0.5$ mW and $P_{\text{r}}/P_{\text{b}} = 1.1$. Also shown are the trap depth distributions for (b) $P_{\text{r}}/P_{\text{b}} = 1.05$ and (d) $P_{\text{r}}/P_{\text{b}} = 1.2$, where the lines on the right sides give the trap potentials along the white dashed lines.

center and the saddle increases with $P_{\text{r}}/P_{\text{b}}$. Conversely, when $P_{\text{r}}/P_{\text{b}}$ is relatively large, the attractive force from red-detuned light increases and the saddle of the trap well moves to the area between the trap center and the waveguide surface, as shown in Fig. 3(d) with $P_{\text{r}}/P_{\text{b}} = 1.2$, $P_{\text{b}} = 0.5$ mW, and $P_{\text{b1}} = 0.1$ mW. The trap potentials along the white dashed lines are given in the right curves in Figs. 3(b) and 3(d). The trap potential on the saddle decreases to form a smaller trap depth as $P_{\text{r}}/P_{\text{b}}$ increases. The saddle moves from infinity to the area between the trap center and the waveguide surface as $P_{\text{r}}/P_{\text{b}}$ increases, which results in a sharp change in the curves for the relation between the trap depth and $P_{\text{r}}/P_{\text{b}}$. It should be noted that excessively large or small $P_{\text{r}}/P_{\text{b}}$ values can diminish the trap depth. A comparison of the various curves clearly reveals that a larger P_{b} results in a greater trap depth. Additionally, the maximum trap depth increases and shifts to the right as P_{b} increases.

The relation between the trap depth and $P_{\text{r}}/P_{\text{b}}$ for different P_{b1} when P_{b} is set equal to 0.5 mW is illustrated in Fig. 3(c), where the different curves correspond to $P_{\text{b1}} = 0.04$, 0.06, 0.08, 0.10, and 0.12 mW. Each curve demonstrates an initial increase in trap depth followed by a decrease as $P_{\text{r}}/P_{\text{b}}$ increases, ultimately reaching a maximum at around $P_{\text{r}}/P_{\text{b}} = 1.14$. A comparison of the different curves reveals that the trap depth increases with P_{b1}. This finding underscores the significant role played by the TM$_{1,\text{b}}$ mode in shaping the trap well and substantially increasing the trap depth. To provide further insight into the TM$_{1,\text{b}}$ mode, the inset of Fig. 3(c) displays the relationship between the trap depth and P_{b1}, with P_{b} set at 0.5 mW and $P_{\text{r}}/P_{\text{b}}$ set at 1.1. This inset graphically depicts the correlation between the trap depth and P_{b1}, showing that the trap depth is very small with very small P_{b1} values. When P_{b1} exceeds 0.01 mW, the trap depth rapidly increases, indicating the significant impact of the TM$_{1,\text{b}}$ mode in enhancing the
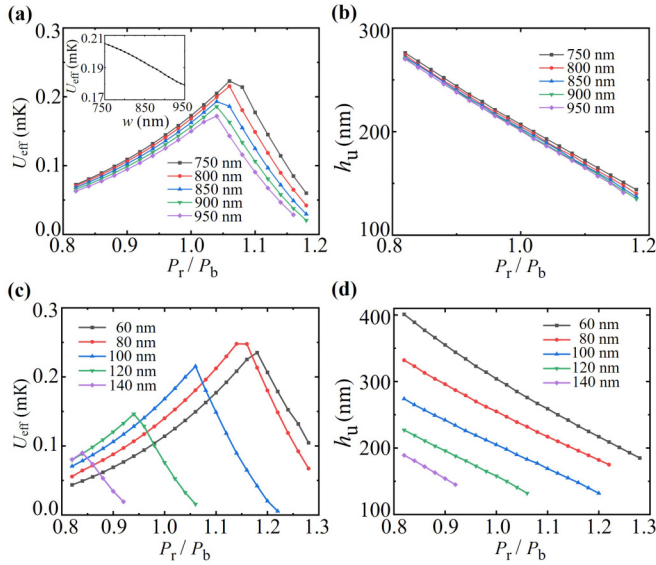
FIG. 4. Relation between the trap depth and P_r/P_b for different waveguide (a) widths w and (c) heights h and relation between the trap center h_u and P_r/P_b for different waveguide (b) widths w and (d) heights h. The inset in (a) shows the relation between the trap depth and the waveguide width w for $P_r/P_b = 1.1$.

trap depth. However, when P_{b1} surpasses 0.1 mW, the curve saturates, signifying that further increases in P_{b1} do not result in an additional trap depth. This suggests that the repair effect of the $TM_{1,b}$ mode ceases to augment the trap depth beyond this point.

The geometry of the waveguide influences the trap depth and trap center location, as shown in Fig. 4, where $P_b = 0.5$ mW and $P_{b1} = 0.1$ mW. In Fig. 4(a), the relationship between the trap depth and the power ratio P_r/P_b is studied for different waveguide widths $w = 750, 800, 850, 900$, and 950 and a fixed height $h = 100$ nm. Different curves indicate that a larger trap depth can be achieved with a smaller waveguide width, because weak confinement leads to a stronger electric field of the SPP mode above the waveguide. The relation between the trap depth and the waveguide width is also evident in the inset of Fig. 4(a) with $P_r/P_b = 1.1$. However, the SPP modes are less effective for forming trap depths either when the waveguide width is greater than 950 nm or when $TM_{1,r}$ is nonexistent when w is less than 750 nm and $h = 100$ nm. In Fig. 4(b), the corresponding relationship between the trap center and P_r/P_b for different waveguide widths is studied, which shows that the waveguide width has little effect on the location of the trap center. In contrast, the ratio P_r/P_b strongly affects the trap center location.

In Fig. 4(c), the relationship between the trap depth and the ratio P_r/P_b is given for different waveguide heights of 60, 80, 100, 120, and 140 nm, with a fixed waveguide width of $w = 800$ nm. The corresponding relationship between the location of the trap center and P_r/P_b for different waveguide heights is also investigated in Fig. 4(d). These results show that both the waveguide height and P_r/P_b have strong effects

on the atom trap potential. A smaller waveguide height allows for a greater distribution of the mode amplitude above the waveguide surface to form the trap well but with a higher trap center. However, it is important to note that the SPP mode experiences significant loss under these conditions. Conversely, with a larger waveguide height, more mode energy is confined within the waveguide, making it challenging to form a well-defined trap well above the waveguide. Therefore, a waveguide width of $w = 800$ nm and a height of $h = 100$ nm are appropriate geometric parameters for the SiO_2 on Au-SiO_2 platform.

V. CONCLUSION

A viable platform utilizing SPP waveguides has been proposed to realize near-field cold-atom trapping with low-power consumption. Specifically, for the SiO_2 waveguide on Au-SiO_2 substrate, a trap depth of 0.239 mK can be achieved with $P_b = 0.5$ mW, $P_{b1} = 0.1$ mW, and $P_r = 0.55$ mW, powers that are almost one order of magnitude lower than those required in dielectric waveguides on a substrate. The trap center is 180 nm above the waveguide surface, allowing enhanced atom-photon interactions with a cooperativity of 0.137. Through manipulation of the phase difference of counterpropagating red-detuned trap lasers in the $TM_{0,r}$ mode, the standing-wave trap well lattice can transport trapped atoms along the waveguide surface. The impacts of the waveguide geometry and trap power on the trap depth were also analyzed. This proposed platform offers a stable and low-power method for realizing atom trapping and strong atom-photon interactions in the short waveguide, which has potential application in the photonic-atomic chip.

[1] J.-H. Kim, S. Aghaeimeibodi, J. Carolan, D. Englund, and E. Waks, Optica **7**, 291 (2020).

[2] A. W. Elshaari, W. Pernice, K. Srinivasan, O. Benson, and V. Zwiller, Nat. Photonics **14**, 285 (2020).

[3] E. Pelucchi, G. Fagas, I. Aharonovich, D. Englund, E. Figueroa, Q. Gong, H. Hannes, J. Liu, C.-Y. Lu, N. Matsuda *et al.*, Nat. Rev. Phys. **4**, 194 (2022).

[4] H. J. Kimble, Nature (London) **453**, 1023 (2008).

[5] F. Grillot, J. Duan, B. Dong, and H. Huang, Light Sci. Appl. **10**, 156 (2021).

[6] W. Luo, L. Cao, Y. Shi, L. Wan, H. Zhang, S. Li, G. Chen, Y. Li, S. Li, Y. Wang *et al.*, Light Sci. Appl. **12**, 175 (2023).

[7] R. Zektzer, N. Mazurski, Y. Barash, and U. Levy, Nat. Photonics **15**, 772 (2021).

[8] F. Davidson-Marquis, J. Gargiulo, E. Gómez-López, B. Jang, T. Kroh, C. Müller, M. Ziegler, S. A. Maier, H. Kübler, M. A. Schmidt *et al.*, Light Sci. Appl. **10**, 114 (2021).

[9] D. E. Chang, J. S. Douglas, A. González-Tudela, C.-L. Hung, and H. J. Kimble, Rev. Mod. Phys. **90**, 031002 (2018).

[10] J.-B. Béguin, A. Burgers, X. Luan, Z. Qin, S.-P. Yu, and H. J. Kimble, Optica **7**, 1 (2020).

[11] L. Chen, C.-J. Huang, X.-B. Xu, Y.-C. Zhang, D.-Q. Ma, Z.-T. Lu, Z.-B. Wang, G.-J. Chen, J.-Z. Zhang, H. X. Tang *et al.*, Phys. Rev. Appl. **17**, 034031 (2022).

[12] Y. B. Ovchinnikov, Appl. Phys. Lett. **120**, 010502 (2022).

[13] J. Lee, R. Ding, J. Christensen, R. R. Rosenthal, A. Ison, D. P. Gillund, D. Bossert, K. H. Fuerschbach, W. Kindel, P. S. Finnegan *et al.*, Nat. Commun. **13**, 5131 (2022).

[14] C. Ropp, W. Zhu, A. Yulaev, D. Westly, G. Simelgor, A. Rakholia, W. Lunden, D. Sheredy, M. M. Boyd, S. Papp *et al.*, Light Sci. Appl. **12**, 83 (2023).

[15] F. Le Kien, V. I. Balykin, and K. Hakuta, Phys. Rev. A **70**, 063403 (2004).

[16] E. Vetsch, D. Reitz, G. Sagué, R. Schmidt, S. T. Dawkins, and A. Rauschenbeutel, Phys. Rev. Lett. **104**, 203603 (2010).

[17] P. Schneeweiss, S. T. Dawkins, R. Mitsch, D. Reitz, E. Vetsch, and A. Rauschenbeutel, Appl. Phys. B **110**, 279 (2013).

[18] A. González-Tudela, C.-L. Hung, D. E. Chang, J. I. Cirac, and H. Kimble, Nat. Photonics **9**, 320 (2015).

[19] M. Gullans, T. G. Tiecke, D. E. Chang, J. Feist, J. D. Thompson, J. I. Cirac, P. Zoller, and M. D. Lukin, Phys. Rev. Lett. **109**, 235309 (2012).

[20] M. E. Kim, T.-H. Chang, B. M. Fields, C.-A. Chen, and C.-L. Hung, Nat. Commun. **10**, 1647 (2019).

[21] S. Yu, J. Lu, V. Ginis, S. Kheifets, S. W. D. Lim, M. Qiu, T. Gu, J. Hu, and F. Capasso, Optica **8**, 409 (2021).

[22] A. Liu, J. Liu, W. Peng, X.-B. Xu, G.-J. Chen, X. Ren, Q. Wang, and C.-L. Zou, Phys. Rev. A **105**, 053520 (2022).

[23] A. Liu, L. Xu, X.-B. Xu, G.-J. Chen, P. Zhang, G.-Y. Xiang, G.-C. Guo, Q. Wang, and C.-L. Zou, Phys. Rev. A **106**, 033104 (2022).

[24] E. Will, L. Masters, A. Rauschenbeutel, M. Scheucher, and J. Volz, Phys. Rev. Lett. **126**, 233602 (2021).

[25] X. Zhou, H. Tamura, T.-H. Chang, and C.-L. Hung, Phys. Rev. Lett. **130**, 103601 (2023).

[26] J. P. Burke, Jr., S.-T. Chu, G. W. Bryant, C. J. Williams, and P. S. Julienne, Phys. Rev. A **65**, 043411 (2002).

[27] T. H. Stievater, D. A. Kozak, M. W. Pruessner, R. Mahon, D. Park, W. S. Rabinovich, and F. K. Fatemi, Opt. Mater. Express **6**, 3826 (2016).

[28] Y. B. Ovchinnikov and F. E. Ayi-Yovo, New J. Phys. **22**, 053003 (2020).

[29] X. Ren, A. Liu, C. Zou, L. Wang, Y. Cai, F. Sun, G. Guo, and G. Guo, Appl. Phys. Lett. **98**, 201113 (2011).

[30] A. Liu, C.-L. Zou, X. Ren, X. Xiong, Y.-J. Cai, H. Liu, F.-W. Sun, G.-C. Guo, and G.-P. Guo, Opt. Express **22**, 23372 (2014).

[31] J. Hong, X. Zhou, R. Zhuang, W. Peng, J. Liu, A. Liu, and Q. Wang, Chin. Opt. Lett. **20**, 023601 (2022).

[32] Z. Chen, Y. Wang, Z. Hou, P. Zhang, and L. Yu, IEEE Sens. J. **22**, 14044 (2022).

[33] D. E. Chang, J. D. Thompson, H. Park, V. Vuletić, A. S. Zibrov, P. Zoller, and M. D. Lukin, Phys. Rev. Lett. **103**, 123004 (2009).

[34] C. Stehle, H. Bender, C. Zimmermann, D. Kern, M. Fleischer, and S. Slama, Nat. Photonics **5**, 494 (2011).

[35] M. Mildner, A. Horrer, M. Fleischer, C. Zimmermann, and S. Slama, J. Phys. B **51**, 135005 (2018).

[36] A. McLachlan, Mol. Phys. **7**, 381 (1964).

[37] S. Y. Buhmann, L. Knöll, D.-G. Welsch, and H. T. Dung, Phys. Rev. A **70**, 052117 (2004).

[38] C.-L. Hung, S. M. Meenehan, D. E. Chang, O. Painter, and H. J. Kimble, New J. Phys. **15**, 083026 (2013).

[39] H. R. Philipp, J. Electrochem. Soc. **120**, 295 (1973).

[40] P. B. Johnson and R.-W. Christy, Phys. Rev. B **6**, 4370 (1972).

[41] E. D. Palik, *Handbook of Optical Constants of Solids* (Academic Press, New York, 1998), Vol. 3.

[42] K. L. Corwin, S. J. M. Kuppens, D. Cho, and C. E. Wieman, Phys. Rev. Lett. **83**, 1311 (1999).

[43] J. D. Thompson, T. Tiecke, N. P. de Leon, J. Feist, A. Akimov, M. Gullans, A. S. Zibrov, V. Vuletić, and M. D. Lukin, Science **340**, 1202 (2013).

[44] X. Zhou, H. Tamura, T.-H. Chang, and C.-L. Hung, Phys. Rev. X **14**, 031004 (2004).

[45] A. Liu, J. Liu, Z. Kang, G.-J. Chen, X.-B. Xu, X. Ren, G.-C. Guo, Q. Wang, and C.-L. Zou, Phys. Rev. A **108**, 033108 (2023).

[46] D. Dai and S. He, Opt. Express **18**, 17958 (2010).

[47] M. J. Maleki and M. Soroosh, Opt. Quantum Electron. **55**, 1266 (2023).

[48] H. Choo, M.-K. Kim, M. Staffaroni, T. J. Seok, J. Bokor, S. Cabrini, P. J. Schuck, M. C. Wu, and E. Yablonovitch, Nat. Photonics **6**, 838 (2012).

[49] P. Shi, G. Zhou, and F. S. Chau, J. Opt. Soc. Am. B **30**, 1426 (2013).